ISSN 0003-701X, Applied Solar Energy, 2019, Vol. 55, No. 5, pp. 315–320. © Allerton Press, Inc., 2019.
Russian Text © The Author(s), 2019, published in Geliotekhnika, 2019, No. 5, pp. 373–380.

SOLAR-ENERGY MATERIALS SCIENCE

Effect of Substrate Temperature on the Physical Properties of $Zn_xSn_{1-x}Se$ Films for Thin-Film Solar Cells

T. M. Razykov[a], K. M. Kuchkarov[a, *], B. A. Ergashev[a], M. Baiev[a], M. Mahmudov[a], R. T. Yuldoshov[a], and A. Nasirov[b]

[a] *Physical–Technical Institute of SPA "Physics–Sun," Uzbekistan Academy of Sciences, Tashkent, 100084 Uzbekistan*
[b] *National University of Uzbekistan, Tashkent, 100174 Uzbekistan*
**e-mail: k.kuchkarov@mail.ru*

Received March 29, 2019; revised May 14, 2019; accepted July 10, 2019

Abstract—At the present time, 92% of the PV market is made using single crystal or polycrystalline wafer silicon. However, producing power with these cells remains expensive compared to conventional power generation. Thin film solar cells have been developed to reduce production costs, especially those based on cadmium telluride (CdTe) and copper indium gallium diselenide (CIGS). Despite a number of successes in the development of thin film solar cells, some problems associated with the toxicity of cadmium and with the high cost of indium and gallium remain, which has prompted researchers to search for alternative materials for solar cells. Novel low cost and high efficiency zinc tin selenide ($Zn_xSn_{1-x}Se$) thin film solar cells are without these drawbacks. However, there is no information in the literature about this new material. The samples of $Zn_xSn_{1-x}Se$ films were fabricated using the chemical molecular beam deposition (CMBD) method at atmospheric pressure in hydrogen flow. ZnSe and SnSe powders with 99.999% purity were used as precursors. The temperature of precursors varied in the range of 850–950°C. Films were deposited at substrate temperature of 500–600°C. Borosilicate glass was used as a substrate. The results showed that the composition of the samples changed toward ZnSe with the temperature of the substrate. The grain size of the samples increased from 2–5 μm to 15–17 μm at substrate temperatures of 500 and 550°C, respectively. At a substrate temperature of 600°C, the grain size decreased to 3–5 μm, which is possibly due to an increase in the ZnSe content. The X-ray diffraction pattern has shown that the samples have ZnSe, SnSe, Se, and Sn phases.

Keywords: $Zn_xSn_{1-x}Se$, X-ray, morphology, grain size, conductivity
DOI: 10.3103/S0003701X19050104

INTRODUCTION

The leading solar cells in the world are solar cells based on wafer silicon and thin films, $Cu(In,Ga,)Se_2$ and CdTe with an efficiency of 26% and 22.0–23.0%, respectively [1–3]. Despite the widespread use of these materials, there are significant restrictions on their use in the global production of photovoltaic modules. For example, the main disadvantage of crystalline silicon-based solar cells is their high cost, since the cost of the Si substrate is 50% of the total cost of these cells. This type of solar cells are made using high-quality raw materials, whose production is currently high energy-intensive. Total losses of silicon as a result of its processing and cutting are large. Due to the fact that monocrystalline and polycrystalline silicon are indirect gap semiconductors, and their absorption coefficient is low, the thickness of the solar cells made of them must be hundreds of microns for effective absorption of sunlight. This leads to significant expenses of silicon and the high cost of solar cells. Meanwhile, for thin-film solar cells based on $Cu(In,Ga,)Se_2$ and CdTe, their further large-scale use is complicated due to the limited reserves of In, Ga, Te in the earth's crust, as well as the toxicity of cadmium (Cd), which is part of the structure of the solar cell.

To achieve a high efficiency of thin-film solar cells, new structures are being developed and studied based on the compounds SnSe, SbSe, $CuSb(S_{1-x}Se_x)_2$, $Cu_2(Sn_{1-x}Ga_x)Se_3$ (CTGS), and Cu_2SnS_3. The elements that make up these structures have a low cost and are non-toxic. These new materials are attractive and have the same properties as $Cu(In, Ga)Se_2$, since their band gap lies in the range of 0.87–1.7 eV [4–10]. The first attempt to obtain film solar cells based on them gave an efficiency result of 4–9.2% [11–19].

Some characteristics of the films of A^2B^6 compounds and their ZnCdS, $(ZnSe)_x(CdTe)_{1-x}$ solid solutions made by chemical molecular beam deposition were considered in [20, 21]. The results obtained in these studies showed that a significant influence on the physical properties of the synthesized solid solu-

Table 1. Energy dispersive X-ray spectroscopy analysis for the $Zn_XSn_{1-X}Se$ films at different substrate temperatures

T_s, °C	ZnSe/SnSe ration in the gas phase	Film composition	Zn, %	Sn, %	Se, %
500	$x = 0.1$	$x = 0.026$	0.85	54.7	54.57
550	$x = 0.1$	$x = 0.04$	2.7	59.4	37.9
600	$x = 0.1$	$x = 0.4$	6.4	58.7	34.9

tion films was exerted by the substrate temperature and their composition.

The physical properties of the new $Zn_xSn_{1-x}Se$ material were first obtained by chemical molecular beam deposition and investigated in our study [22]. The further optimization of the technological parameters of these materials requires detailed studies of their structural and electrical properties, depending on the temperature of the substrate. The results of these studies are presented in this paper.

EXPERIMENT

The preparation of solid solution films II–VI using the CMBD method was described in detail in [23]. SnSe and ZnSe powders of purity (99.999%), which evaporated in hydrogen flow at atmospheric pressure, were used as the precursor material. The temperature range of the precursors was 850–950°C, and the substrate temperature varied in the range of 500–600°C. The hydrogen carrier gas flow was ~20 cm^3/min. The duration of the deposition process depended on the required film thickness and ranged from 30 to 60 min. Borosilicate glasses were used as substrates.

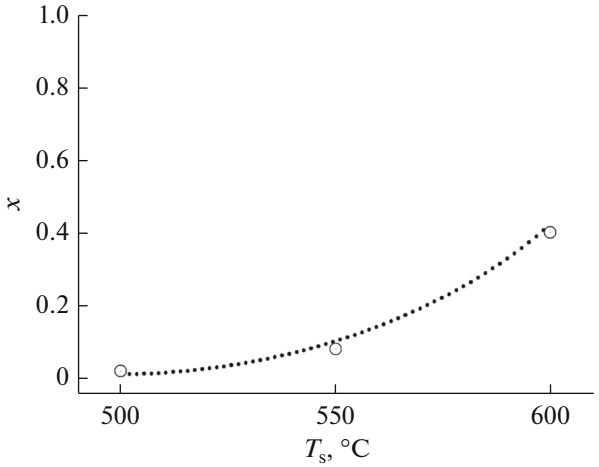

Fig. 1. Dependence of the composition of $Zn_xSn_{1-x}Se$ films on substrate temperature.

X-ray studies of the samples were performed on a Panalytical Empyrean X-ray diffractometer (CuK_α = 1.5406 Å). The measurements were carried out at room temperature in the range of angles 2θ from 20° to 80°. Morphological studies were carried out using a SEM-EVO MA 10 scanning electron microscope; film compositions were determined using an energy-dispersive elemental analyzer of the EDX brand (Oxford Instrument) – Aztec Energy Advanced X-act SDD.

Silver-ohmic contacts were applied to as deposited films by vacuum deposition to carry out electrical measurements. The resistivity of the samples was determined using the van der Pauw method; the type of conductivity of the samples was determined by the thermo-EMF sign. The film thickness (up to 0.5–3 μm) was determined on a MII-4 microinterferometer, as well as by precision micro-weighing on an FA 120 4C balance (with an accuracy of 0.1mg).

RESULTS AND DISCUSSION

The results of energy-dispersive analysis showed (Table 1) that the deposited $Zn_xSn_{1-x}Se$ solid solution films had different compositions at substrate temperatures of 500, 550, and 600°C: $x = 0.026$ at 500°C, $x = 0.04$ at 550°C, and $x = 0.4$ at 600°C.

In the case of a decrease the temperature of the substrate, the condensation of tin vapor on the contrary begins to prevail. Meanwhile, zinc vapors, not reaching the substrate, sublimate in a higher temperature zone on the walls of the reactor and, therefore, the composition of the films shifts toward an increase in the content of the narrow-gap SnSe component, which is described more detail in [23]. This is due to the fact that thermal stability, sublimation heat, and lattice formation energy for binary compounds are directly proportional to the band gap.

Figure 2 shows X-ray diffraction patterns for the $Zn_xSn_{1-x}Se$ solid solution films at various substrate temperatures. The main peaks in the X-ray diffraction pattern were the peaks, which corresponded to the (400), (600) and (800) planes. The total intensity of the peaks of the (400), (600), and (800) planes for the

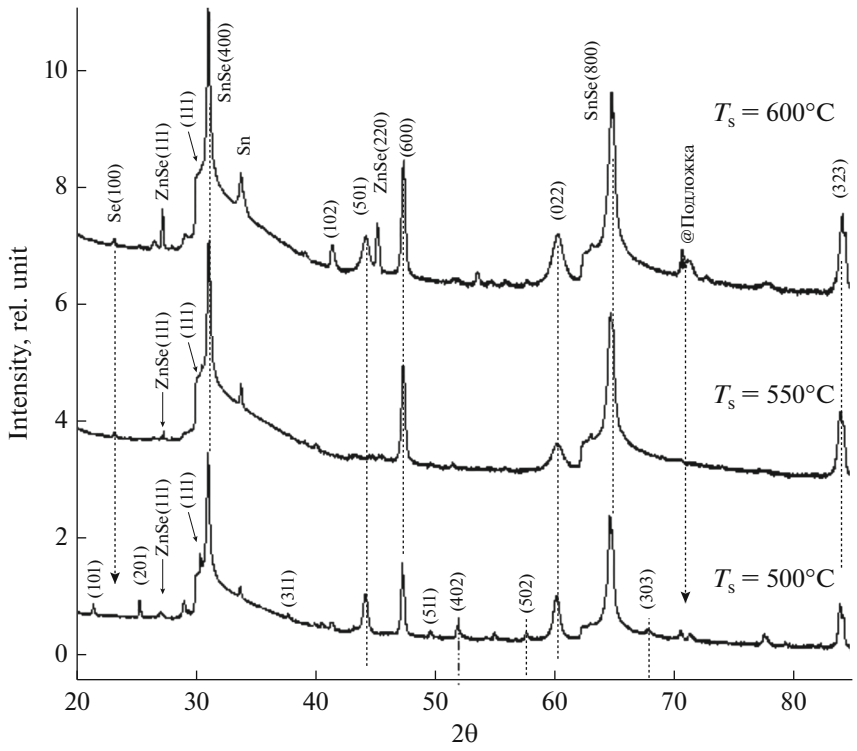

Fig. 2. X-ray diffraction patterns of $Zn_xSn_{1-x}Se$ films at different substrate temperatures.

samples was 90–95% of the intensity of all the peaks of the $Zn_xSn_{1-x}Se$ films in the X-ray diffraction pattern. Along with the peaks of the indicated planes, the X-ray diffraction patterns of the samples also contained peaks corresponding to the (101), (100), (111), (311), (501), (200), (511), (402), (502), (022), and (323) planes, whose intensity was extremely low in comparison with the intensities of the main (400), (600) and (800) peaks. The additional peaks shown in the spectrum are due to the glass substrate, on which the film was grown. The peaks corresponding to oxide phases were not observed.

As can be seen from the X-ray diffraction pattern, almost all the observed peaks of the $Zn_xSn_{1-x}Se$ solid solution films correspond to the SnSe and ZnSe phases. A low intensity reflex is also observed at 34.75°, indicating the formation of the Sn phase [24].

As shown in Fig. 2, all the observed peaks of the $Zn_xSn_{1-x}Se$ solid solution films slightly increased with increasing substrate temperature. This may be due to different thicknesses of $Zn_xSn_{1-x}Se$ films. An increase in the intensities of the two peaks that correspond to the (111) and (200) planes with an increase in the substrate temperature is associated with a growth in the molar content of the wide-gap component (ZnSe).

According to the results of X-ray diffraction analysis, the films had orthorhombic and cubic structures. The crystal lattice parameters for the samples were calculated using the following formula:

$$\frac{1}{d^2} = \frac{h^2}{a^2} + \frac{k^2}{b^2} + \frac{l^2}{c^2},$$

where d is the distance between the planes, and h, k, l are the Miller indices. The lattice parameters of the films at a substrate temperature of 500°C had the following values: a = 11.487 Å, b = 4.215 Å, c = 4.471 Å; at 550°C they had values a = 11.475 Å, b = 4.214 Å, c = 4.473 Å, and at 600°C they had values of a = 11.467 Å, b = 4.205 Å, c = 4.485 Å, respectively. The structural parameters of $Zn_xSn_{1-x}Se$ solid solution films are presented in Table 2. As can be seen, the values of the crystal lattice parameters "a" and "b" for the $Zn_xSn_{1-x}Se$ solid solution films decrease with increasing substrate temperature, and the value of "c" increases. Peak shifts are observed on the X-ray diffraction pattern. Figure 3 shows the (400) peak. A shift of the maximum towards an increase in 2θ indicates a decrease in the interplanar spacing and lattice parameters, respectively.

Figure 4 shows the images obtained by the scanning electron microscope for all samples deposited at various substrate temperatures. Microcrystals for all the $Zn_xSn_{1-x}Se$ solid solution films are uniformly distributed over the surface of the substrate. As can be seen from Fig. 4, the microstructure (shape and grain size)

Table 2. Structural parameters of the $Zn_xSn_{1-x}Se$ films

T_s, °C	Film composition	2θ	(*h k l*)	Grain size, Å	*d*, Å	Parameters of the constant lattice, Å
500	$x = 0.026$	25.3	201	28120	3.72	$a = 11.487$, $b = 4.215$, $c = 4.471$
		27.14	111	12056	3.23	
		30.04	111	28765	2.935	
		31.05	400	28968	2.871	
		44.2	501	1299	2.04	
		47.4	600	3316	1.9	
		60.26	022	228	1.51	
		64.86	800	4886	1.45	
		67.9	303	3.9	1.3	
550	$x = 0.04$	23.2	100	28493	3.8	$a = 11.475$, $b = 4.214$, $c = 4.473$
		27.14	111	28718	3.2	
		30.04	111	28700	2.93	
		31.05	400	2647	2.868	
		60.26	022	594	1.5	
		64.86	800	5595	1.44	
		70.8		905	1.33	
		84.02	323	685	1.15	
600	$x = 0.4$	23.2	100	826	3.7	$a = 11.467$, $b = 4.205$, $c = 4.485$
		27.14	111	11092	3.2	
		30.04	111	28505	2.93	
		31.05	400	28975	2.864	
		44.2	501	1299	2.04	
		45.14	220	2659	2.0	
		47.4	600	11646	1.9	
		60.26	202/022	513	1.53	
		64.86	800	1329	1.43	
		70.8		1438	1.33	

of the samples depends on the temperature of the substrate. When substrate temperature grew, the grain shape of the films did not change, and the grain size increased. Meanwhile, the grain shapes of all samples deposited at temperatures of 500, 550, and 600°C were densified. The grain sizes for all samples were 2–15 μm and had a polycrystalline structure, but the grain sizes of the films deposited at a substrate temperature of 550°C increased to 8–20 μm, and the structure became more densely packed, while the grain size of the films deposited at a substrate temperature of 600°C decreased. This may be due to an increase in the molar fraction of ZnSe.

The electrical parameters of the $Zn_xSn_{1-x}Se$ films (σ, E_{ac} and conductivity type) are given in Table 3. As can be seen, when the temperature of the substrate increased, the electrical conductivity of the $Zn_xSn_{1-x}Se$ films obtained at $T_s = 500$ and 550°C changed insignificantly, and at $T_s = 600$°C it decreased significantly and amounted to $\sigma = 1 \times 10^{-6}$ (Ohm cm)$^{-1}$. Meanwhile, an inversion of the conductivity type of the solid

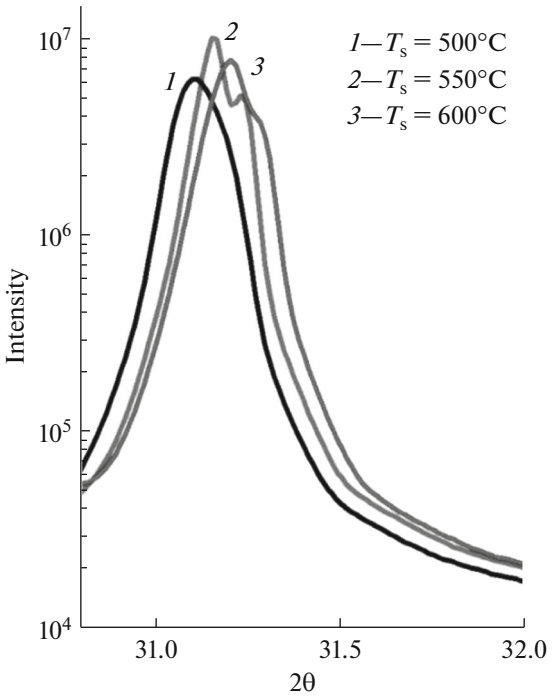

Fig. 3. Shift of the peak (400) of X-ray patterns for $Zn_xSn_{1-x}Se$ films.

solution films was detected; in the case of an increase in the temperature of the substrate, namely, at $T_s = 500$ and 550°C, the samples had *p*-type conductivity, and at $T_s = 600$°C they had *n*-type conductivity. A significant decrease in the electrical conductivity of the $Zn_xSn_{1-x}Se$ solid solution films at $T_s = 600$°C is due to an increase in the molar content of the wide-gap ZnSe component. The highest value $\sigma = 1 \times 10^2$ (Ohm cm)$^{-1}$ of the $Zn_xSn_{1-x}Se$ films was observed at $T_s = 500$°C.

CONCLUSIONS

The $Zn_xSn_{1-x}Se$ solid solution films were obtained by chemical molecular beam deposition at atmospheric pressure of a hydrogen flow, at various substrate temperatures, in the range of 500–600°C. Investigated their morphological, structural and electrical properties.

The results of energy dispersive analysis have shown that the deposited $Zn_xSn_{1-x}Se$ solid solution films at substrate temperatures of 500, 550 and 600°C have different compositions: $x = 0.026$ at 500°C, $x = 0.04$ at 550°C, and $x = 0.4$ at 600°C, respectively.

The data of the scanning electron microscope and X-ray diffraction analysis have shown the following: (1) the films have an orthorhombic and cubic polycrystalline structure; (2) the grain size of the films is 2–20 microns.

The experimental results of measuring the electrical properties of the samples have shown that the electrical conductivity of the $Zn_xSn_{1-x}Se$ solid solution films significantly decreased at $T_s = 600$°C and had an *n*-type con-

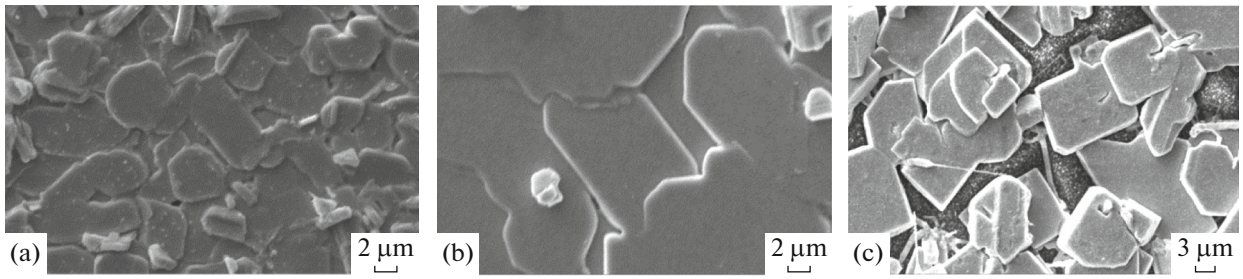

Fig. 4. SEM images of $Zn_xSn_{1-x}Se$ films at different substrate temperatures. (a) $T_s = 500$°C; (b) $T_s = 550$°C; and (c) $T_s = 600$°C.

Table 3. Electrical parameters of $Zn_xSn_{1-x}Se$ film

T_s, °C	Films deposited from the ZnSe and SnSe compounds with the stoichiometric composition			
	film composition	σ, (Ohm cm)$^{-1}$	$E_{activation}$, eV	conductivity type
500	$x = 0.026$	100	0.02	*p*
550	$x = 0.04$	25	0.04	*p*
600	$x = 0.4$	1×10^{-6}	0.22	*n*

ductivity. The highest value of $\sigma = 1 \times 10^2$ (Ohm cm)$^{-1}$ of the $Zn_xSn_{1-x}Se$ films was observed at $T_s = 500$°C.

An inversion of the conductivity type was observed: the samples obtained at substrate temperatures of 500, 550°C were of *p*-type, and at a temperature of 600°C they had *n*-type of conductivity.

The results make it possible to manufacture new and cheap solar cells based on these materials.

ACKNOWLEDGMENTS

This work was carried out within the FA-F3-003 project at the Physical-Technical Institute of the Uzbekistan Academy of Sciences.

REFERENCES

1. Jäger-Waldau, A., Veneri, P.D., Bosio, A., et al., Recent progress in photovoltaics, Part 1, *Sol. Energy,* 2018, vol. 175, pp. 1–110.
2. Jackson, P., Wuerz, R., and Hariskos, D., Effects of heavy alkali elements in $Cu(In,Ga)Se_2$ solar cells with efficiencies up to 22.6%, *Phys. Status Solidi,* 2016, vol. 8, pp. 583–586. https://doi.org/10.1002/pssr.201600199
3. First Solar Sets Record for CdTe Solar PV Efficiency, 2016. http://solarbuzz.com/industry-news/first-solar-sets-record-cdte-solar-pv-efficiency.
4. Sanchez, F. de B. and Nair, M.T.S., Optimum chemical composition of antimony sulfide selenide for thin film solar cells, *Appl. Surf. Sci.,* 2018, vol. 454, pp. 305–312.
5. Razykov, T.M., Boltaev, G.S., Bosio, A., et al., Characterisation of SnSe thin films fabricated by chemical molecular beam deposition for use in thin film solar cells, *Sol. Energy,* 2018, vol. 159, pp. 834–840.
6. Meng, M., Wan, L., Zou, P., et al., $Cu_2ZnSnSe_4$ thin films prepared by selenization of one-electrochemically deposited Cu–Zn–Sn–Se precursors, *Appl. Surf. Sci.,* 2013, vol. 273, pp. 613–616.
7. Kumar, V. and Sinha, A., Concentration and temperature dependence of the energy gap in some binary and alloy semiconductors, *Infrared Phys. Technol.,* 2015, vol. 69, pp. 222–227.
8. Suresh Babu, G., Kishore Kumar, Y.B., Bharath Kumar Reddy, Y., and Sundara Raja, V., Growth and characterization of Cu_2SnSe_3 thin films, *Mater. Chem. Phys.,* 2006, vol. 96, pp. 442–446.
9. Takei, K., Maeda, T., and Wada, T., Crystallographic and optical properties of $CuSbS_2$ and $CuSb(S_{1-x}Se_x)_2$ solid solution, *Thin Solid Films,* 2015, vol. 582, pp. 263–268.
10. Reddy, V. and Reddy, M., Perspectives on SnSe-based thin film solar cells: a comprehensive review, *J. Mater. Sci.,* 2016, vol. 27, no. 6, pp. 5491–5508.
11. Chen, Z., Guo, X., Guo, H., and Ding, J., Fabrication of a semi-transparent thin-film Sb_2Se_3 solar cell, *Mater. Lett.,* 2019, vol. 236, pp. 503–505.
12. Zhang, G.H., Boix, P.P., Wong, L.H., et al., Towards high efficiency thin film solar cells, *Prog. Mater. Sci.,* 2017, vol. 87, pp. 246–291.
13. Abd El-Rahman, K.F., Darwish, A.A.A., and El-Shazly, E.A.A., Electrical and photovoltaic properties of SnSe/Si heterojunction, *Mater. Sci. Semicond. Proces.,* 2014, vol. 25, pp. 123–129.
14. Li, J., Xue, C., and Wang, Y., Cu_2SnS_3 solar cells fabricated by chemical bath deposition–annealing of SnS/Cu stacked layers, *Sol. Energy Mater. Sol. Cells,* 2016, vol. 144, pp. 281–288.
15. Umehara, M., Takeda, Y., and Tajima, Sh., Improvement of red light response of $Cu_2Sn_{1-x}Ge_xS_3$ solar cells by optimization of CdS buffer layers, *J. Appl. Phys.,* 2015, vol. 118, p. 154.
16. He, M., Kim, J., and Suryawanshi, M.P., Influence of sulfurization temperature on photovoltaic properties of Ge alloyed Cu_2SnS_3(CTGS) thin film solar cells, *Sol. Energy Mater. Sol. Cells,* 2018, vol. 174, pp. 94–101.
17. Wen, X., Chen, Ch., Lu, Sh., and Kanghua, Vapor transport deposition of antimony selenide thin film solar cells with 7.6% efficiency, *Nat. Commun.,* in press. https://doi.org/10.1038/s41467-018-04634-6
18. Li, Z., Liang, X., Li, G., and Haixu, 9.2%-efficient core-shell structured antimony selenide nanorod array solar cells, *Nat. Commun.,* in press.doi.org/10.1038/s41467-018-07903-6
19. Shinde, D.V., Min, S.-K., Sung, M., et al., Photovoltaic properties of nanocrystalline SnSe–CdS, *Mater. Lett.,* 2014, vol. 115, pp. 244–247.
20. Razykov, T.M., Physical properties of $Zn_xCd_{1-x}S$ films obtained by chemical vapor deposition in a hydrogen stream, *Geliotekhnika,* 1984, no. 6, pp. 13–16.
21. Razykov, T.M., Kadyrov, B.Kh., and Khodyaeva, M.A., Energy band models of *n*-Zn_xCd_{1-x}S-p-CdTe and *n*-$Zn_xCd_{1-x}S$–*p*-Si heterojunctions, *Phys. Status Solidi,* 1985, vol. 91, pp. 87–91.
22. Razykov, T.M., Kuchkarov, K.M., Ergashev, B.A., et al., Production and characteristics of $(ZnSe)_{0.1}(SnSe)_{0.9}$ films for use in thin film solar cells, *Appl. Sol. Energy,* 2017, vol. 54, no. 4, pp. 255–260.
23. Razykov, T.M., Physical properties of II–VI binary and multicomponent compound films and heterostructures fabricated by chemical vapour deposition, *Thin Solid Films,* 1988, vol. 164, pp. 301–308.
24. Shikha, D., Jeewan, V.M., and Sharma, R.P., Electrical characterization of nanocrystalline SnSe and ZnSe thin films: effect of annealing Deep, *J. Mater. Sci.: Mater. Electron.,* 2018, vol. 29, pp. 13614–13619.

Translated by L. Solovyova